

NUMERICAL SIMULATION OF THE SUPERSONIC FLOW OVER A TWO-DIMENSIONAL WEDGE-RECTANGLE

Roberto Francisco Bobenrieth Miserda

Universidade de Brasília – Departamento de Engenharia Mecânica
Campus Universitário Darcy Ribeiro – Asa Norte – Brasília, DF – 70910-900
roberto@enm.unb.br

Alessandra Freire de Mendonça

Universidade de Brasília – Departamento de Engenharia Mecânica
Campus Universitário Darcy Ribeiro – Asa Norte – Brasília, DF – 70910-900
afmend@zipmail.com.br

***Abstract.** This work is a first step toward the large-eddy simulation of finite wedge-rectangle. In this work, the test case is a semi-infinite wedge-rectangle, composed by adjoining a finite wedge with a semi-infinite rectangle. For this geometry, analytic results for the normal shock are available for detached shocks and the same kind of results are available for the attached oblique shock and the isentropic expansion produced by the wedge-rectangle geometry. These analytical results are obtained considering the flow as inviscid, and for this reason, a full slip condition is imposed in the wedge-rectangle wall. The numerical results agree very well with the analytical ones in almost all the simulated Mach numbers.*

***Keywords.** supersonic flow, wedge-rectangle, detached shock, oblique shock, Prandtl-Meyer expansion*

1. Introduction

This work is a first step toward the large-eddy simulation of the supersonic flow over a finite wedge-rectangle. The large-eddy simulation of complex compressible flows, with strong interaction between shock and turbulent wakes, is still a challenge for the scientific community. Even in simple configurations, this kind of flows undergoes rapid changes such as dramatic amplifications of turbulence levels after the shock and loss of isotropy. There are few examples of this kind of work (Garnier et al., 2002). In this context, it is mandatory to validate the compressible code with analytical results for supersonic flows in order to separate the effects of steady-state compressible flow from compressible, time dependant, large-eddy effects.

In this work, the test case is a semi-infinite wedge-rectangle, composed by adjoining a finite wedge with a semi-infinite rectangle. For this geometry, analytic results for the normal shock are available for detached shocks and the same kind of results are available for the attached oblique shock and the isentropic expansion produced by the adjoining wedge-rectangle geometry. These analytical results are obtained considering the flow as inviscid, and for this reason, a full slip condition is imposed in the wedge-rectangle wall. With this boundary conditions and geometry, the sub-grid turbulence model will act solely as a numerical viscosity, controlling the numerical oscillations induced by the strong gradients across the shock. The numerical results obtained are compared with the analytical results available for each simulated Mach number.

2. Mathematical model and numerical method

Since this work is a first step toward the large-eddy simulation of the flow in a finite two-dimensional wedge-rectangle, the mathematical model used in this work is for the large-scale field. To obtain the large-scale field, the equations of continuity, momentum, and energy are filtered using the classical “box” filter (Clark et al., 1979). The resulting equations are (Garnier et al., 2002)

$$\frac{\partial \bar{\rho}}{\partial t} + \frac{\partial}{\partial x_i} (\bar{\rho} \tilde{u}_i) = 0 \quad (1)$$

$$\frac{\partial}{\partial t} (\bar{\rho} \tilde{u}_i) + \frac{\partial}{\partial x_j} (\bar{\rho} \tilde{u}_i \tilde{u}_j) = - \frac{\partial \bar{p}}{\partial x_i} + \frac{\partial}{\partial x_j} [(\tilde{\mu} + \mu_t) \tilde{S}_{ij}] \quad (2)$$

$$\frac{\partial}{\partial t}(\bar{\rho} \tilde{e}_i) + \frac{\partial}{\partial x_i}(\bar{\rho} \tilde{e}_i \tilde{u}_i) = -\frac{\partial}{\partial x_i}(\bar{p} \tilde{u}_i) + \frac{\partial}{\partial x_i}[(\tilde{\mu} + \mu_t) \tilde{S}_{ij} \tilde{u}_j] + \frac{\partial}{\partial x_i} \left[\left(\tilde{k} + \frac{k_t}{\gamma} \right) \frac{\partial \tilde{T}}{\partial x_i} \right] \quad (3)$$

The straight over bar refers to the filtered variable using the “box” filter and the curved one refers to the filtered variable using the Favre filter (Anderson et al., 1984). This filter is based in the “box” filter and results in a filtered variable weighted by the density, defined as

$$\tilde{\phi} = \overline{\rho \phi} / \bar{\rho} \quad (5)$$

The other symbols as their usual meanings, i.e., x_i is the spatial coordinate in the i direction, t is the temporal coordinate, ρ is the density, u_i is the component of the velocity in the i direction, p is the pressure, T is the temperature, μ is the molecular dynamic viscosity and S_{ij} is the viscous-strain tensor, given by

$$\tilde{S}_{ij} = \left(\frac{\partial \tilde{u}_i}{\partial x_j} + \frac{\partial \tilde{u}_j}{\partial x_i} \right) - \frac{2}{3} \delta_{ij} \frac{\partial \tilde{u}_k}{\partial x_k} \quad (6)$$

It is important to note that the second term of the viscous-strain tensor is a function of the divergence of the vector field that physically represents the time rate of change of the volume of a moving fluid element, per unit volume. This term will be especially high when the fluid element passes through a shock wave. The specific total energy (total energy per unit mass), e_t , is calculated as

$$\tilde{e}_t = \tilde{e} + \tilde{e}_k = \tilde{e} + \frac{\tilde{u}_i \tilde{u}_i}{2} \quad (7)$$

where e and e_k represents the specific internal and kinetic energy, respectively. The working fluid is air, considered a calorically and thermally perfect gas. In this case, the relation between the temperature and the specific internal energy is given by

$$\tilde{T} = \frac{(\gamma - 1)}{R} \tilde{e} \quad (8)$$

where γ is the specific heats ratio and R is the gas constant. Air is also considered a perfect gas, so the state equation is

$$\bar{p} = \bar{\rho} R \tilde{T} \quad (9)$$

and the molecular dynamic viscosity is given by the Sutherland law (Schlichting, 1968):

$$\tilde{\mu} = \tilde{T}^{3/2} \left(\frac{1 + C}{\tilde{T} + C} \right) \quad (10)$$

where $C = 0,4$, which corresponds to a reference temperature of 276 K.

The effect of the sub-grid scales is accounted using the Smagorinsky (1963) sub-grid model, where the turbulent dynamic viscosity is given by

$$\mu_t = \bar{\rho} (C_s A)^2 \sqrt{2 \tilde{S}_{ij} \tilde{S}_{ij}} \quad (11)$$

It is important to note that the turbulent viscosity will have a non-zero value in the shock waves, due to the dependence of the viscous-strain tensor, \tilde{S}_{ij} , on the divergence of the vector field, as mentioned above. This implies that the introduction of a sub-grid model will affect the flow in the shock waves, making mandatory a comparison between the numerical and analytical results in order to evaluate how the sub-grid model affects the flow. The relation between the turbulent viscosity and the turbulent conductivity, k_t , is obtained using the turbulent Prandtl number, Pr_t , in the form

$$k_t = \frac{c_p}{Pr_t} \mu_t \quad (11)$$

The boundary conditions at the wall of the wedge-rectangle used in this work is full slip. This boundary condition is imposed in order to compare the numerical results with the analytical results for the normal shock, oblique shock and the Prandtl-Meyer expansion. It is important to note that these analytical results were obtained considering an inviscid flow. For this reason, it is important to emulate this restriction using a full slip condition at the wall. Otherwise, a boundary layer will be generated, and its presence will slightly alter the results since the potential flow will see a slightly different wedge-rectangle. The mathematical model represented by Eq. (1) to Eq. (11) is solved using MacCormack's (1969) explicit predictor-corrector algorithm in its finite volume formulation. This method has a second-order precision in space and time.

3. Numerical implementation

Figure (1) presents a detail of the computational grid used in all cases. It is important to notice that only 1/6 of the wedge surface is shown. The angle θ of the wedge is 18.43° , resulting from the relation 1/3 between the height and the length of the wedge. The former size is 0.1 m and the last is 0.3 m. The adjoining rectangle has the same height and its length is 9.7 m. The origin was located at the leading edge of the wedge. The grid extends from the points (-2.0, 0.0) to (98.0, 1.0) in the direction of the flow, containing 650 control volumes, and from the points (-2.0, 0.0) to (-2.0, 100.0) in the direction normal to the flow, also containing 650 control volumes. The region of regular mesh is contained between the points (-2.0, 0.0), (7.0, 1.0), (-2.0, 10.0) and (7.0, 10.0), with 450 control volumes in the direction of the flow and 500 control volumes in the direction normal to the flow.

The total number of control volumes is 422,500, with 225,000 located in the regular-mesh region, resulting in a problem with 1,690,000 degrees of freedom. The code was run in an AMD Athlon 1.33 GHz workstation, with a mean of 1.5 CPU seconds per iteration. A typical run consisted in 30,000 iterations, resulting in 12.5 hours of CPU time.

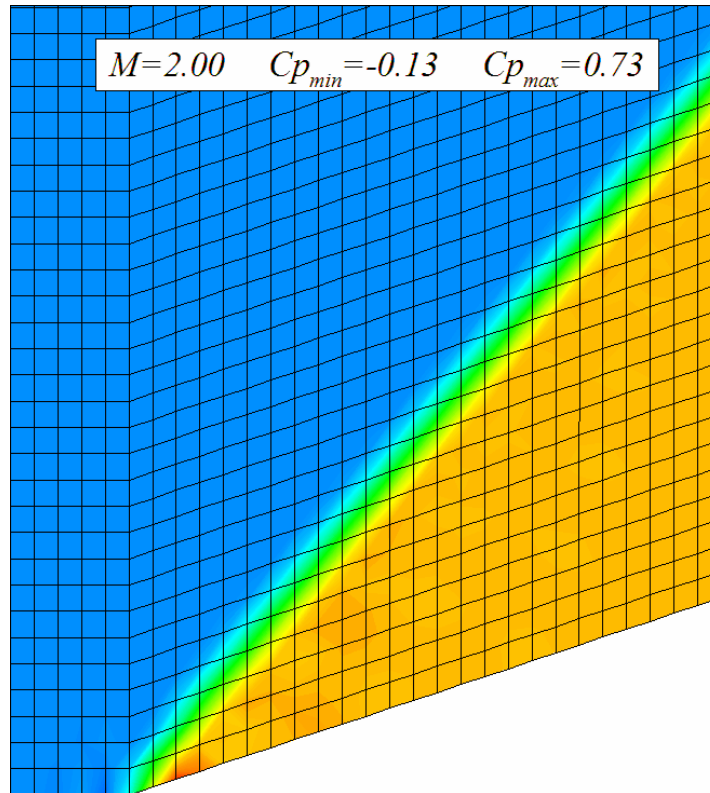


Figure 1. Detail of the computational grid used for all cases. Only 1/6 of the wedge surface is shown. The oblique shock for $M_\infty = 2.0$ appears in the background.

4. Results

The code was run for six different Mach numbers: 1.5, 1.65, 1.8, 2.0, 2.6 and 5.0. From the analytical solution, based on the $\theta - \beta - M$ relation (Anderson, 1990) and given by

$$\tan \theta = 2 \cot \beta \left[\frac{M^2 \sin^2 \beta - 1}{M^2 (\gamma + \cos 2\beta) + 2} \right] \quad (12)$$

it can be seen that for the first two Mach numbers the shock must be detached, since the value of $\theta = 18.43^\circ$ is greater than the value of θ_{\max} given by the $\theta - \beta - M$ diagram. For the other four Mach numbers, the shock is oblique and attached, since value of $\theta = 18.43^\circ$ is lesser than the value of θ_{\max} given by the same diagram. Figures (2), (4), (6), (8), (10) and (12) show the pressure coefficient field, C_p , given by

$$C_p = \frac{2(p - p_\infty)}{\rho_\infty U_\infty^2}. \quad (13)$$

In this work, the values of the undisturbed thermodynamics properties used are $p_\infty = 101,300$ Pa and $T_\infty = 300$ K.

In Figs. (2) and (4), the shock is clearly detached and in Figs. (6), (8), (10) and (12), the shock is oblique and attached. It can be seen from the $\theta - \beta - M$ diagram that the transition value for the Mach number, from detached to attached, is approximately 1.77. This value that is between $M_\infty = 1.65$, corresponding to Fig. (4), and $M_\infty = 1.80$, corresponding to Fig. (6). In Tab. (1) are presented the shock angle β at the symmetry line for numerical (N) and analytical (A) results for different Mach numbers. This angle is calculated graphically from Figs. (2), (4), (6), (8), (10) and (12). The analytical value for Figs. (2) and (4) is 90.0° , since the shock is detached. The analytical values for Figs. (6), (8), (10) and (12) are calculated using $\theta - \beta - M$ diagram.

In Tab. (2) are presented the pressure coefficient at compression (C_{p_c}) and expansion (C_{p_e}) for numerical and analytical results for different Mach numbers. The numerical values were obtained from Figs. (3), (5), (7), (9), (11) and (13). In this figures, the value of C_p shown are in the upwind symmetry line (from $x = -2.0$ to $x = 0.0$), the wedge wall (from $x = 0.0$ to $x = 3.0$) and the adjoining rectangle wall (from $x = 3.0$ to $x = 7.0$). The analytical results for the pressure coefficient at compression (C_{p_c}) were obtained using the normal shock relations for the Mach numbers $M_\infty = 1.50$ and $M_\infty = 1.65$ (since the shock is detached) and $\theta - \beta - M$ diagram for the other Mach numbers (since the shock is attached and oblique). The analytical results for the pressure coefficient at expansion (C_{p_e}) over the adjoining rectangle were obtained using the Prandtl-Meyer function (Anderson, 1990), given by

$$\nu(M) = \sqrt{\frac{\gamma+1}{\gamma-1}} \tan^{-1} \sqrt{\frac{\gamma-1}{\gamma+1} (M^2 - 1)} - \tan^{-1} \sqrt{M^2 - 1}. \quad (14)$$

It is important to mention that only in the case of attached oblique shocks it is possible to calculate analytically the properties after the expansion using the Prandtl-Meyer function, since the value of the properties remain constant over the wedge wall only in the case of the attached shock, as shown in Figs. (7), (9), (11) and (13). In Figs. (3) and (5), it can be seen that after the normal shock at the symmetry line, all properties change along the flow direction.

Tables (3) and (4) present the numerical and analytical results for the nondimensional temperature and Mach number at compression and expansion, respectively. The methodology for obtaining the analytical results is identical to the one use to generate Tab. (2). The numerical results were extracted from figures for nondimensional temperature and Mach number, similar to Figs. (3), (5), (7), (9), (11) and (13), that are not presented in this work, due to space limitations.

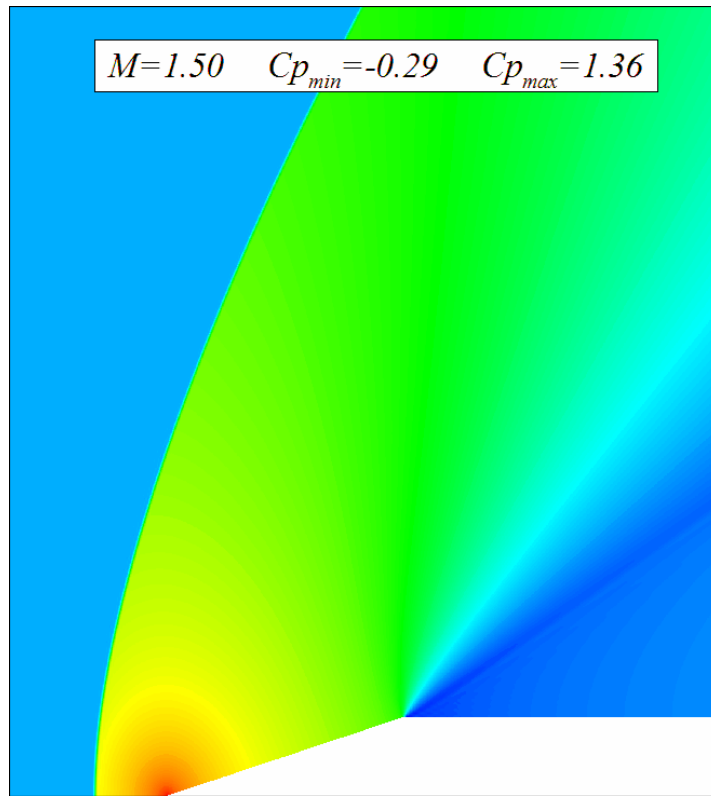


Figure 2. C_p field for $M_\infty = 1.50$. Maximum value corresponds to red and minimum to blue.

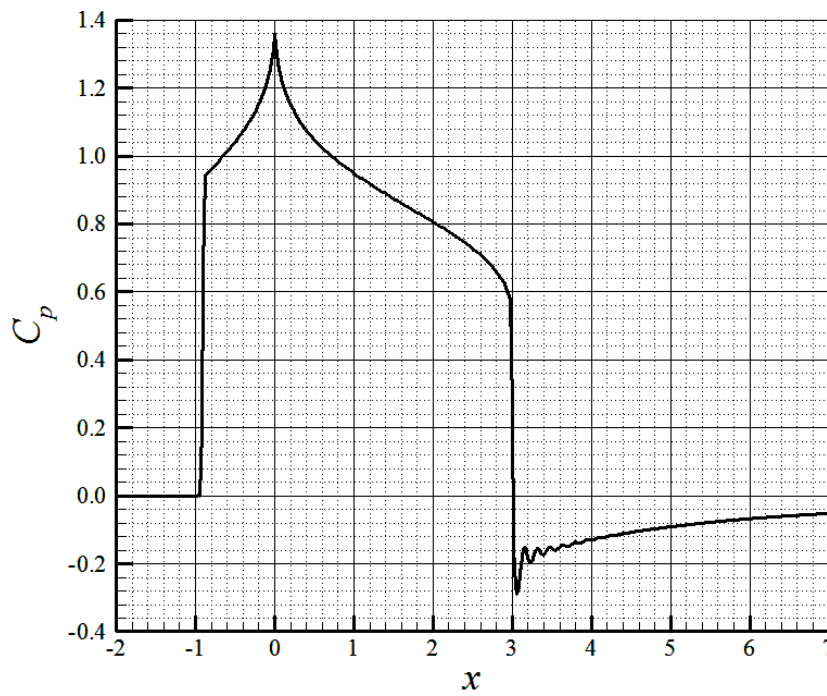


Figure 3. C_p values for $M_\infty = 1.50$ over the symmetry line ($y = 0$) and over the wedge-rectangle surface.

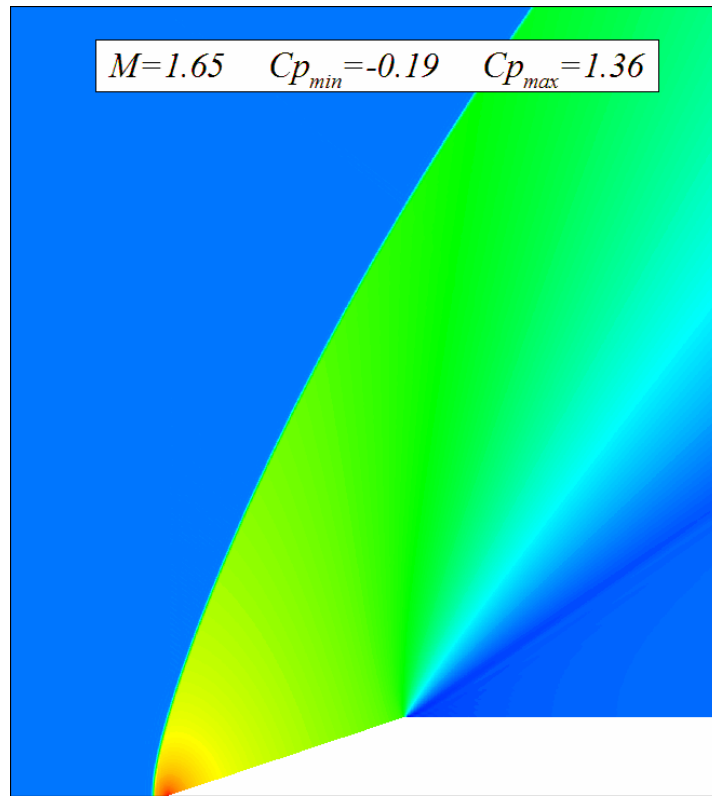


Figure 4. C_p field for $M_\infty = 1.65$. Maximum value corresponds to red and minimum to blue.

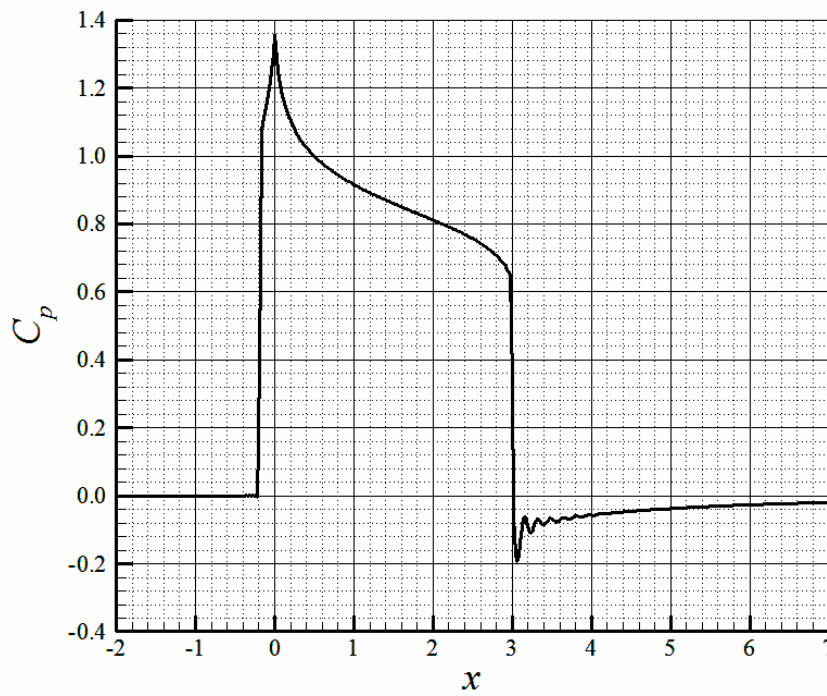


Figure 5. C_p values for $M_\infty = 1.65$ over the symmetry line ($y = 0$) and over the wedge-rectangle surface.

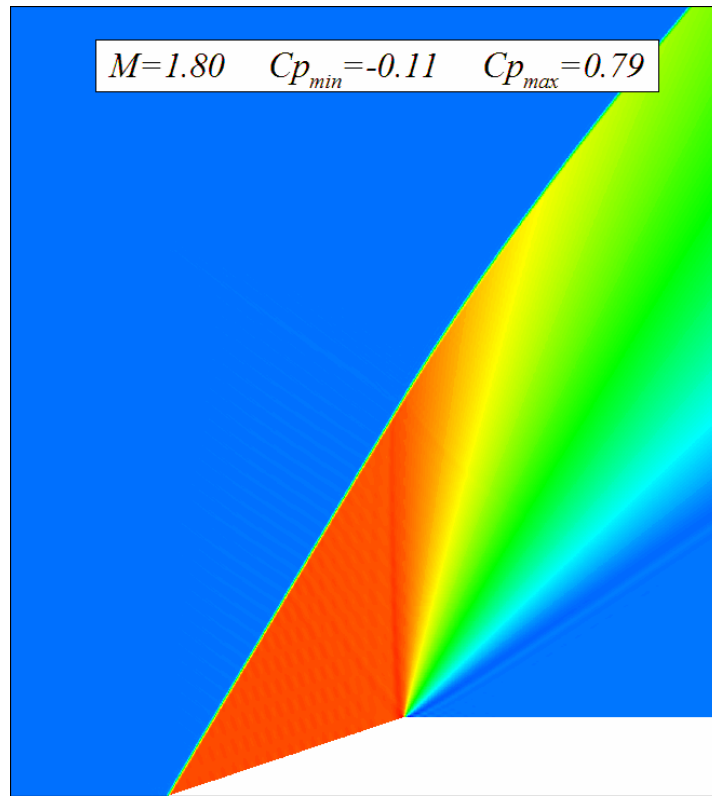


Figure 6. C_p field for $M_\infty = 1.80$. Maximum value corresponds to red and minimum to blue.

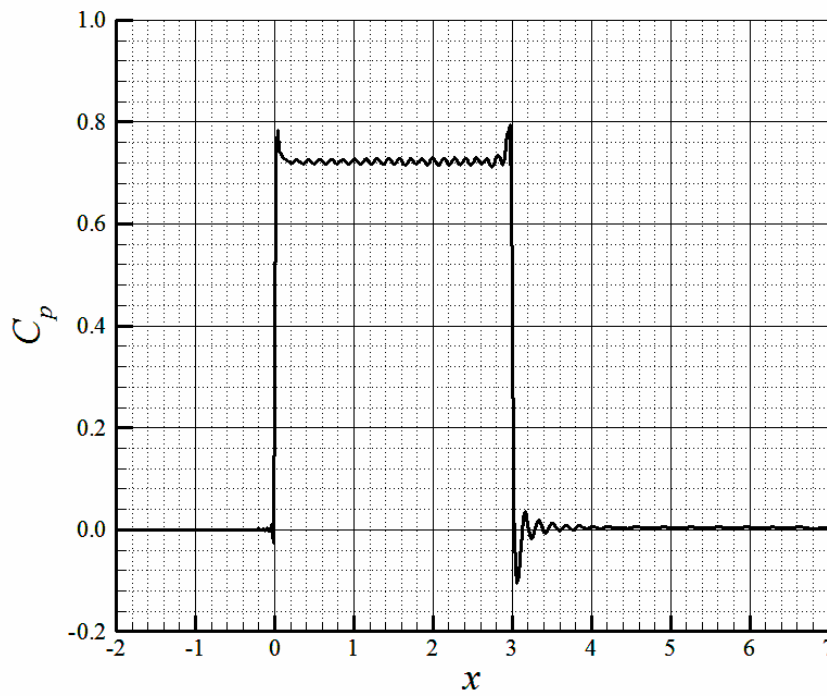


Figure 7. C_p values for $M_\infty = 1.80$ over the symmetry line ($y = 0$) and over the wedge-rectangle surface.

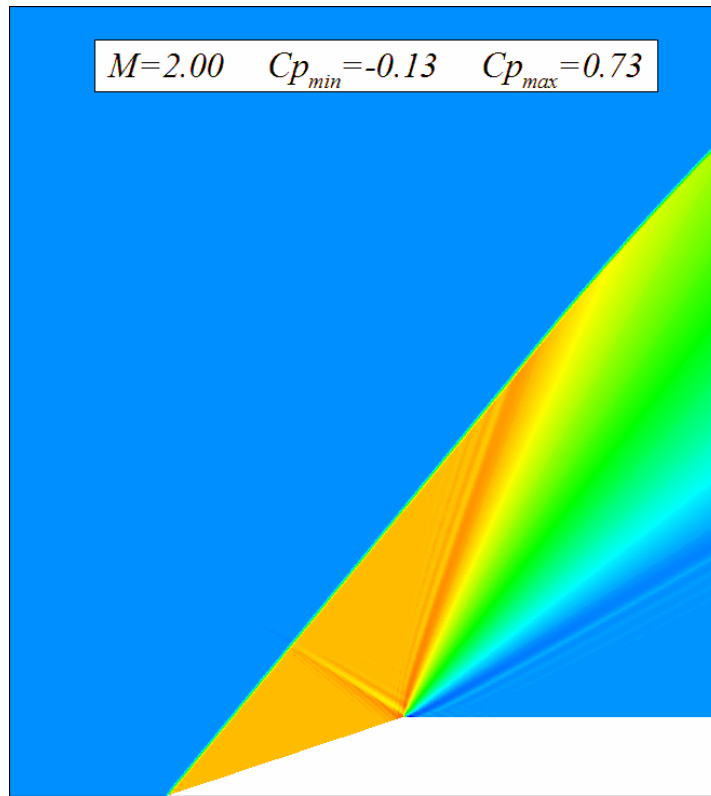


Figure 8. C_p field for $M_\infty = 2.00$. Maximum value corresponds to red and minimum to blue.

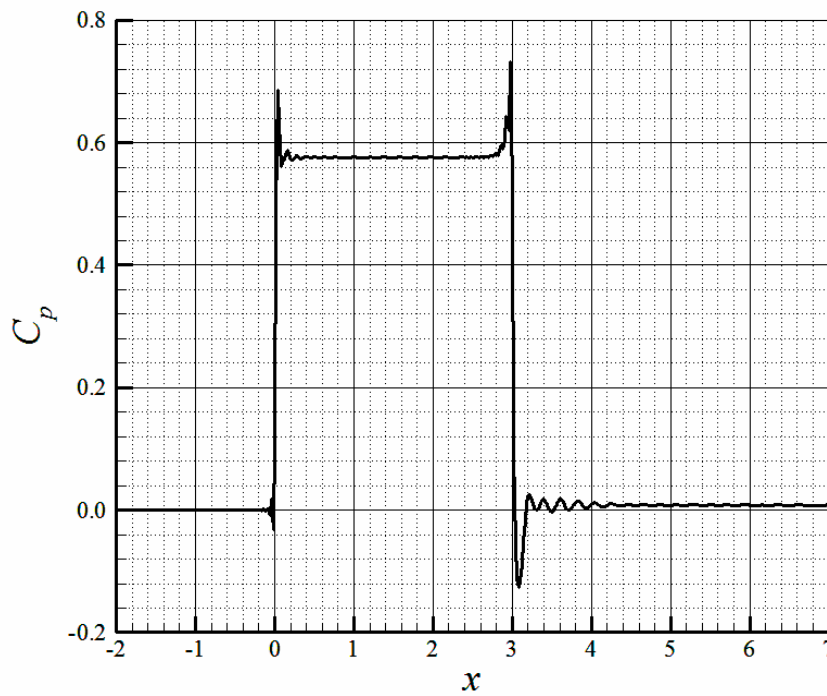


Figure 9. C_p values for $M_\infty = 2.00$ over the symmetry line ($y = 0$) and over the wedge-rectangle surface.

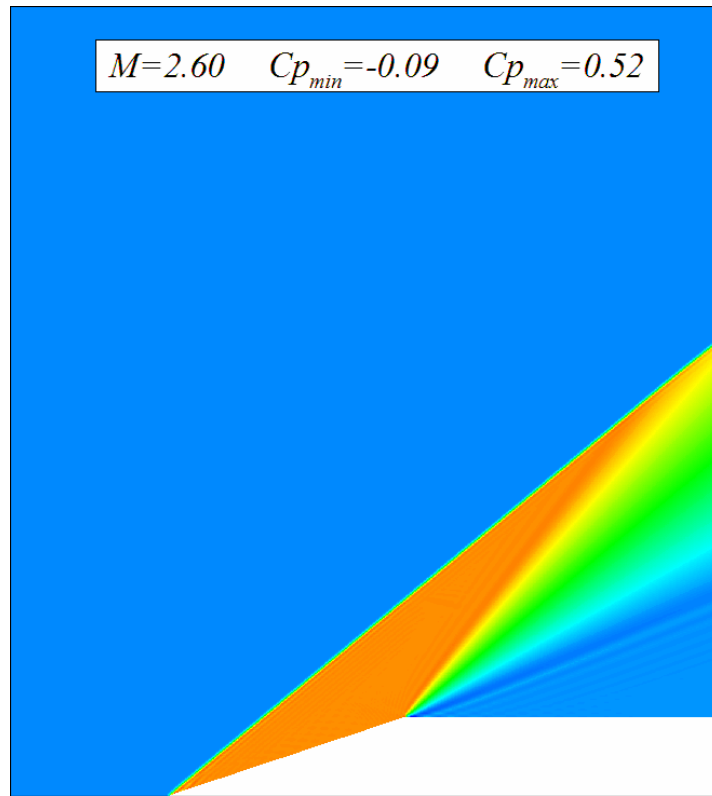


Figure 10. C_p field for $M_\infty = 2.60$. Maximum value corresponds to red and minimum to blue.

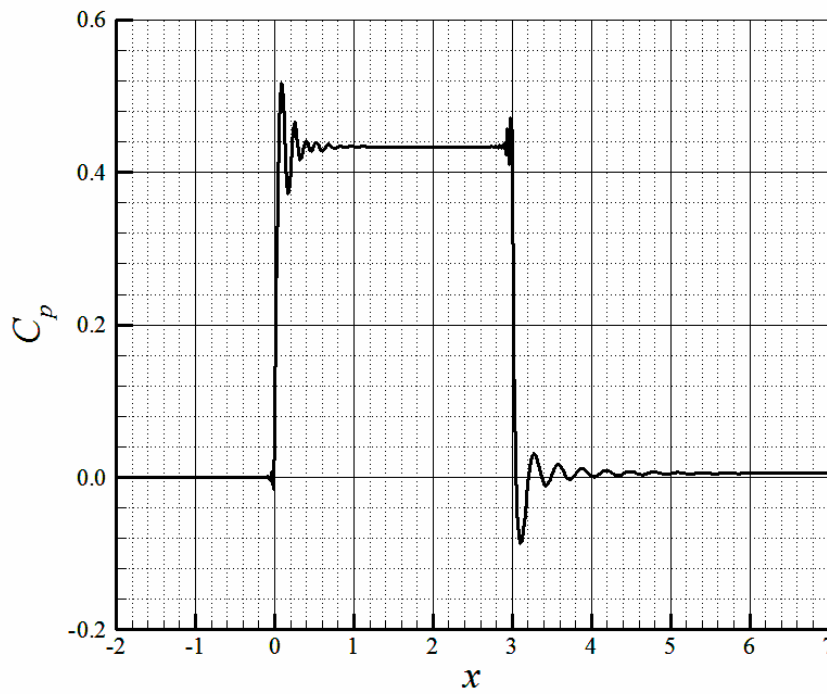


Figure 11. C_p values for $M_\infty = 2.60$ over the symmetry line ($y = 0$) and over the wedge-rectangle surface.

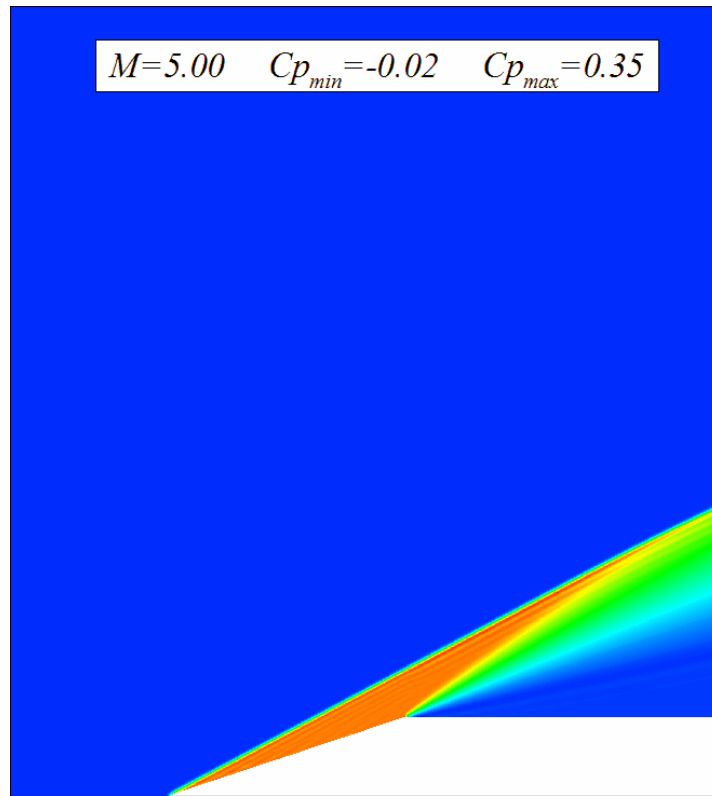


Figure 12. C_p field for $M_\infty = 5.00$. Maximum value corresponds to red and minimum to blue.

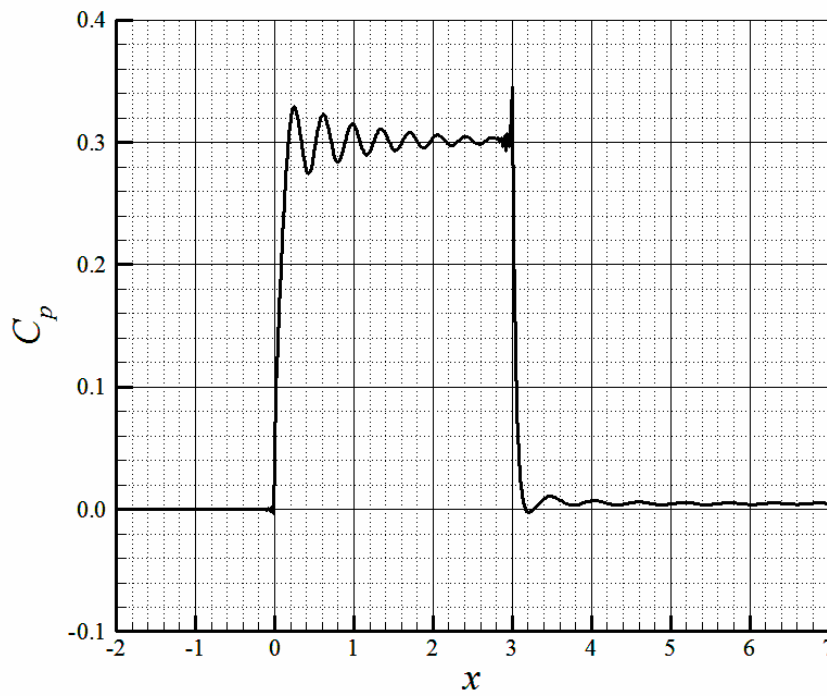


Figure 13. C_p values for $M_\infty = 5.00$ over the symmetry line ($y = 0$) and over the wedge-rectangle surface.

Table 1. Shock angle at the symmetry line for numerical (N) and analytical (A) results for different Mach numbers.

| M_∞ | β_N | β_A | $\varepsilon(\beta)$ |
|------------|-----------|-----------|----------------------|
| 1.50 | 90.0° | 90.0° | 0.00% |
| 1.65 | 90.0° | 90.0° | 0.00% |
| 1.80 | 59.1° | 59.2° | -0.12% |
| 2.00 | 50.0° | 50.7° | -1.38% |
| 2.60 | 39.9° | 39.6° | +0.76% |
| 5.00 | 28.1° | 28.0° | +0.36% |

 Table 2. Pressure coefficient at compression and expansion for numerical (N) and analytical (A) results for different Mach numbers.

| M_∞ | $(C_{PC})_N$ | $(C_{PC})_A$ | $\varepsilon(C_{PC})$ | $(C_{PE})_N$ | $(C_{PE})_A$ | $\varepsilon(C_{PE})$ |
|------------|--------------|--------------|-----------------------|--------------|--------------|-----------------------|
| 1.50 | 0.9456 | 0.9257 | +2.15% | - | - | - |
| 1.65 | 1.0921 | 1.0545 | +3.57% | - | - | - |
| 1.80 | 0.7178 | 0.7154 | +0.34% | 0.0030 | 0.0028 | +0.03% |
| 2.00 | 0.5757 | 0.5815 | -1.00% | 0.0082 | -0.0039 | +2.07% |
| 2.60 | 0.4335 | 0.4306 | +0.67% | 0.0053 | 0.0041 | +0.28% |
| 5.00 | 0.2986 | 0.3007 | -0.70% | 0.0046 | 0.0027 | +0.64% |

 Table 3. Nondimensional temperature at compression and expansion for numerical (N) and analytical (A) results for different Mach numbers.

| M_∞ | $(T_C/T_\infty)_N$ | $(T_C/T_\infty)_A$ | $\varepsilon(T_C/T_\infty)$ | $(T_E/T_\infty)_N$ | $(T_E/T_\infty)_A$ | $\varepsilon(T_E/T_\infty)$ |
|------------|--------------------|--------------------|-----------------------------|--------------------|--------------------|-----------------------------|
| 1.50 | 1.3258 | 1.3259 | -0.01% | - | - | - |
| 1.65 | 1.4347 | 1.4230 | +0.82% | - | - | - |
| 1.80 | 1.3612 | 1.3513 | +0.73% | 1.0544 | 1.0278 | +2.58% |
| 2.00 | 1.3490 | 1.3524 | -0.25% | 1.0561 | 1.0230 | +3.24% |
| 2.60 | 1.4198 | 1.4280 | -0.57% | 1.0665 | 1.0453 | +2.03% |
| 5.00 | 2.0018 | 1.9906 | +0.56% | 1.3790 | 1.2037 | +14.56% |

 Table 4. Mach number at compression and expansion for numerical (N) and analytical (A) results for different Mach numbers.

| M_∞ | $(M_C)_N$ | $(M_C)_A$ | $\varepsilon(M_C)$ | $(M_E)_N$ | $(M_E)_A$ | $\varepsilon(M_E)$ |
|------------|-----------|-----------|--------------------|-----------|-----------|--------------------|
| 1.50 | 0.6882 | 0.7011 | -1.84% | - | - | - |
| 1.65 | 0.6231 | 0.6540 | -4.72% | - | - | - |
| 1.80 | 1.0428 | 1.0481 | -0.51% | 1.6790 | 1.7371 | -3.34% |
| 2.00 | 1.2871 | 1.2867 | +0.03% | 1.8734 | 1.9232 | -2.59% |
| 2.60 | 1.8004 | 1.7988 | +0.09% | 2.4541 | 2.5002 | -1.84% |
| 5.00 | 3.1322 | 3.1734 | -1.30% | 4.1796 | 4.4635 | -6.36% |

6. Conclusions

The variable ε that appears in Tabs. (1), (2), (3) and (4) represent the relative error between the numerical and analytical values. These last values were obtained using the normal shock relations for the detached shock, and the $\theta - \beta - M$ diagram and the Prandtl-Meyer function for the oblique attached shock. From an inspection of these tables it can be concluded that the numerical results agree very well with the analytical ones in almost all the simulated Mach numbers, since the maximum relative error is around 3%. The only exception is for $M_\infty = 5.00$, where the maximum relative error is 14.56% for the temperature at the expansion. But, it is important to note that this high level of error occurs only at the expansion and only for the temperature and Mach number (that strongly depends on the temperature). For this Mach number the results for the pressure coefficient are very good. This fact can be explained looking at Figs. (12) and (13). It can be observed a high level of numerical oscillation after the compression and the expansion. It must be noted that the value of the Smagorinsky constant used in all the other Mach numbers is $C_S = 0.5$, and this value is enough to maintain the numerical stability of the code. In the other hand, a value of $C_S = 0.8$ was necessary to maintain the numerical stability for $M_\infty = 5.00$. This is a direct result of the high level of inclination of the oblique shock for the fixed grid used in this work, shown in Fig. (1). From the results presented in this work, it can be concluded that the

introduction of sub-grid scale model affects the code in a positive way, augmenting its numerical stability and reducing the oscillations that are typical of second-order methods. This can be clearly seen in Figs. (3) and (5), where the normal part of the detached shocks has no oscillations at all. In the later case, $M_\infty = 1.65$, the shock strength is the higher of all cases analyzed. This is a direct result of the numerical viscosity also being a function of the divergence of the velocity field, which has a non-zero value in the shock. As it was mentioned above, the numerical oscillations that are observed in the case of the oblique attached shocks are function of the inclination of the shock in relation to the grid. There is no relative inclination in Figs. (3) and (5) up to the value $\alpha = 0.0$. This problem can be solved using a grid that conforms better to the geometry of the shock, reducing in this way the relative inclination between them. Finally, it is concluded that the code is ready for the next phase of this work, which is the large-eddy simulation of a finite wedge-rectangle, due to the fact that the introduction of a sub-grid model affects the code in the positive ways described above. A preliminary result of this phase is presented in Fig. (14).

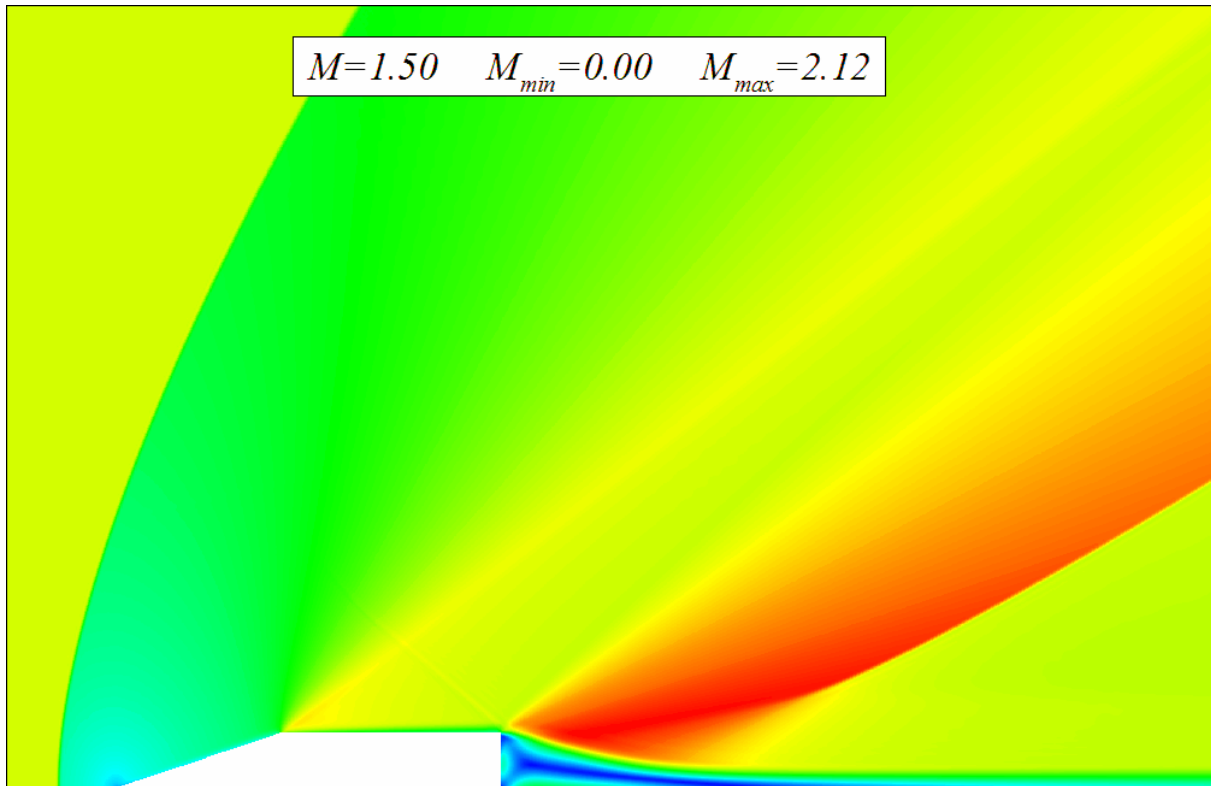


Figure 14. Preliminary results for the large-eddy simulation of a finite wedge-rectangle.

7. References

- Anderson, D.A., Tannehill, J.C., Pletcher, R. H., 1984, "Computational Fluid Mechanics and Heat Transfer", Hemisphere Publishing Corporation, New York, 599 p.
- Anderson, J.D., 1990, "Modern Compressible Flow", Mac-Graw Hill, Inc., New York, 650 p.
- Clark, R.A., Ferziger, J.H., Reynolds, W.C., 1979, "Evaluation of Subgrid-Scale Models using an Accurately Simulated Turbulent Flow", J. Fluid Mech., Vol. 91, pp. 1-16.
- Garnier, E., Sagaut, P., Deville, M., 2002, "Large Eddy Simulation fo the Shock/Homogeneous Turbulence Interaction", Computers & Fluids, Vol. 31, pp.245-268.
- MacCormack, R.W., 1969, "The effect os Viscosity in the Hipervelocity Impact Cratering", AIAA Paper 69-354, Cincinnati, Ohio.
- Schlichting, H., 1968, "Boundary-Layer Theory", McGraw-Hill Book Company, New York, 376 p.